Data Assimilation with ROMS-LETKF

for the Coastal Ocean

Ying Zhang

A scholarly paper in partial fulfillment of the requirements for the degree of

Master of Science

February 2019

Department of Atmospheric and Oceanic Science, University of Maryland

College Park, Maryland

Advisor: Dr. Kayo Ide

Contents

ABSTRACT

The coastal ocean is one of the most critical regions of the ocean. It has many unique and complex physical processes spanning various spatial and temporal scales. The central California coast is one of such areas. It has significant coastal upwelling processes, involving mesoscale eddies and fronts. It is also a well-sampled area where a variety of observations are made though a number of field experiments. To better understand the physical processes and improve the estimation and prediction in the this area, an advanced ensemble Kalman filter method coupled with the Regional Ocean Modeling System (ROMS) for the central California coast is used in this study. This study focuses on two aspects in data assimilation (DA): stratification of coastal ocean and dynamic constraints, under the observing system simulation experiments (OSSEs) framework in an idealized California current system.

1. Introduction

1.1. Coastal Ocean System

The coastal ocean is one of the most critical regions of the ocean, which has high socio-economic value due to recreation, shipping, fisheries, and mineral/oil/gas exploitation. In addition, its complex and unique physical characteristics due to the control of surface and bottom boundaries and coastlines, biological, and biogeochemical processes have drawn increasing attention to scientists in many fields. With the growing concern in the coastal ocean, real-time monitoring and forecasting are vital and have been emphasized. The observations of the coastal ocean are usually inhomogeneous and sporadic in space and time; an ocean model and an advanced data assimilation (DA) system are thus necessitated.

In this study, the central California coast is our concern, which has interesting dynamics spanning a wide range of spatial and temporal scales. The typical phenomenon in this region is coastal upwelling process, characterized by a tens-of-kilometers wide cold band along the coast. Southward winds drive offshore Ekman transport, force surface waters offshore, and draw deeper colder water to the surface. Mesoscale eddies and fronts are observed to separate the cold upwelling region and warm offshore area. The upper ocean in the offshore area has strong stratification supported by surface heating. The central California coast is also one of the well-sampled ocean regions. A number of field experiments have been carried out there and a variety of observations from different observing platforms with various density and coverage are available, such as data from shallow-water gliders, moorings and high-frequency (HF) radar (Chao et al. 2009). Hence, these valuable observations provide us with a possibility to improve our understanding of dynamical processes in this region and model simulations and predictions through DA systems.

This research aims at building a DA system based on an advanced ensemble Kalman filter (EnKF) scheme in a regional ocean model (see Section 2.1). In the meanwhile, we also hope this research can help the design and development of observing systems in the California coastal area. The reason of selecting an EnKF as a DA system is its ability of considering the flow-dependent information and then estimating time-evolving forecast error covariance by an ensemble of model runs. The advanced EnKF method that we are using is the Local Ensemble Transform Kalman Filter (LETKF) by Hunt et al. (2007). More details of the LETKF will be shown in Section 2.2. The LETKF has recently been used in coastal ocean data assimilation and promising results were found in the observing system simulation experiments (OSSEs) in the Chesapeake Bay (Hoffman et al. 2012). In this study, we focus on two aspects associated with the DA system: stratification of coastal ocean and dynamic constraints. Other aspects that can potentially have significant impact including multiscale DA schemes and the assimilation of HF radar radial velocity are also discussed.

1.2.1) Stratification

Vertical stratification of the ocean due to the water masses with different densities is a naturally occurring phenomenon and the ocean is separated by several layers with different properties in the vertical. An ocean DA system is expected to properly handle the vertical stratification.

In an ensemble-based Kalman filtering DA system, the time-evolving background error covariance is estimated in the ensemble space. Due to the limit of the computational and storage resources, the ensemble size is typically small and could not be infinitely increased to a comparable number of degrees of freedom in numerical models. Hence, the ensemble-based background error covariance suffers from rank deficiency and spurious correlations between distant locations (e.g. Hacker et al. 2007; Hunt et al. 2007); the analysis is then negatively

affected by the observations far way in a random manner (Hunt et al. 2007). In addition, Patil et al. (2001) found that the spatiotemporally chaotic atmosphere has low dimensionality in local regions. This local low-dimensionality feature allows the feasibility that the analysis could be obtained in high-dimensional space if local analysis could choose different linear combinations of the ensembles in different local regions (Hunt et al. 2007). In practice, "space localization" is introduced to localize the observational influences on the state variables nearby, suppress the spurious correlations and ameliorate sampling errors in the EnKF with a finite number of ensemble members. Besides improving the DA performance, the "space localization", in which the local analysis could be calculated independently, allows the implementation of efficient parallel computation (Keppenne 2000; Keppenne and Rienecker 2002; Hunt et al. 2007).

The "space localization" method is typically carried out by applying a distance-dependent function, which decays to zero beyond a distance, to either the background error covariance (namely the B localization in Greybush et al. 2011) or the observation error covariance (namely the R localization in Greybush et al. 2011). For instance, Hamill et al. (2001) used an elementwise multiplication of the background error covariance matrix with a correlation function with local support to reduce noisiness and then improve background error covariance estimate. Hunt et al. (2007) multiplied the inverse observation error covariance by a Gaussian function that decays from one to zero as the distance of the observations from the analysis grid point increases. Other types of the "space localization" have also been designed, such as a hierarchical ensemble filter by which Anderson (2007) used to adaptively estimate the sampling error and the impact of spurious sample correlations between an observation and model state variables.

Many studies of the "space localization" are done in horizontal directions (e.g. Houtekamer and Mitchell 1998; Hamill et al. 2001; Greybush et al. 2011); while a few consider the localization in the vertical (e.g. Houtekamer et al. 2005; Whitaker et al. 2004; Keppenne and Rienecker 2002; Hacker et al. 2007). For atmospheric DA, Houtekamer et al. (2005) applied

the Schur product and Whitaker et al. (2004) employed a covariance filter to background error covariance to confine the horizontal and vertical impact of observations in atmospheric EnKF methods. For ocean DA, Keppenne and Rienecker (2002) used a Hadamard product with a three-dimensional canonical correlation function to limit spurious covariances in the background error covariances in a multivariate EnKF with the Poseidon ocean circulation model. Penny et al. (2013) applied a Gaussian weighting in the vertical to a constant cutoff distance in order to limit the influence of observations far way from the analysis grid point in their recent work of four-dimension LETKF coupled with the Geophysical Fluid Dynamics Laboratory Modular Ocean Model 2.2. Cummings (2005) reviewed three options of vertical correlation length-scales in the correlation of background error covariance in ocean DA: (i) constant, (ii) monotonically increasing or decreasing with depth, or (iii) changing with background vertical density gradients. Vertical correlation length scales could be evolved from analysis cycles.

Because of the stratification, the influence of observations that are collected within the mixed layer should be localized in the mixed layer and observations that are made in the deep ocean will not be used in the mixed layer. In addition, the ocean is more sampled in the upper layers than beneath in the vertical. Therefore, the vertical localization associated with stratification is important for ocean DA.

1.2.2) Dynamic Constraints

The state of ocean in numerical models is described by several relationships: the equation of state, temperature-salinity ($T - S$) relation, and geostrophic and thermal wind balance. During DA processes, the analysis is computed as an optimal combination of a short-range forecast from numerical models (i.e. background) and recent observations. The background variables that are outputted from numerical models usually comply with the dynamic balance underlying in the models; whereas different types of observations with different error are not dynamically consistent. Once a variety of observations are assimilated, the analysis may not

sustain the reasonable dynamic balances as the background. As a result, the forecast that is integrated from the analysis will degrade rapidly. In addition, background error covariance with better cross-variable correlation through dynamic constraints usually leads to better dynamically balanced analyses in a multivariate system (Weaver et al. 2005). Therefore, dynamic constraints are crucial in DA systems.

Dynamic constraints can be fulfilled through either a post process after univariate DA or being involved in background error covariance in multivariate DA. Troccoli et al. (2002) assimilated temperature observations only, updated salinity increments using temperature analysis based on the model $T - S$ relationship and achieved better forecasts of the mean state and temporal variability compared with experiments without constraints. However, this kind of approach is apparently not valid for assimilating different types of observations. Ricci et al. (2005) assimilated both temperature and salinity, included $T - S$ constraint within the background error covariance in a 3DVar system and found not only significant improvements of the salinity mean state but also remove spurious geostrophic currents in univariate analysis. More general and complex methods are exploited to incorporate multivariate dynamic constraints. Weaver et al. (2005) introduced a method from Derver and Bouttier (1999) into incremental variational DA coupled with an ocean general circulation model (OGCM). In this paper, a multivariate balance operator was designed to transform model background error covariance from model space of highly-correlated variables to a control space of approximately uncorrelated nondimensional control variables. All state variables except for temperature are divided into balanced and unbalanced parts. Temperature is used to build the balanced part of other variables based on geostrophy, hydrostatic and dynamic height balance and linearized $T - S$ relationship and equation of state. For coastal area, the background error covariance is significantly inhomogeneous and anisotropic and thus special treatment is needed. Li et al. (2008) utilized two dynamic constraints, hydrostatic and geostrophic balance, to the increments in their ROMS3DVAR system. The model state variables were also separated into balanced and unbalanced parts based on two con-

straints. Moreover, nonhomogeneous and anisotropic ageostrophic velocity were substituted by ageostrophic streamfunction and velocity potential in order to avoid non-zero cross-error covariance of ageostrophic velocity. Hence the background error covariance was constructed by nonsteric sea surface height, ageostrophic streamfunction and velocity potential, and temperature and salinity. Particularly, for multiscale DA schemes, the MS-3DVar formulation introduced by Li et al. (2012) flexibly incorporates different dynamic balance for different decorrelation length scales.

Dynamic constraints are usually considered in variational DA framework, as shown in aforementioned studies. However, they are rarely emphasized in EnKF-based DA schemes. In this prospectus, we would like to investigate the dynamic balance associated with stratification in the LETKF scheme.

The ultimate goal is to establish an LETKF-based simulating/predicting system that can address strong stratification, dynamic constraints, multiscale dynamic processes and multiscale observations, especially HF radar radial velocity off the central California coast. Such a system is expected to have better performance than the current operational 3DVar system in the central California coast.

2. Methodology

2.1. Model Description - ROMS

The ocean model used in this study is the Regional Ocean Modeling System (ROMS) (Shchepetkin and McWilliams 2005, 2008) developed by the University of California, Los Angeles (UCLA). The UCLA-ROMS model has been widely used for a variety of applications in coastal oceans, such as simulating circulation (Capet et al. 2004, 2008a,b,c), biogeochemical processes (Gruber et al. 2006) and sediment transport (Blaas et al. 2007) in the ocean.

ROMS is built on incompressible, hydrostatic, and three-dimensional primitive equations. It allows free-surface elevation and uses the full equation of state based on potential temper-

ature and density. It solves the equations by using innovative algorithms for time-stepping, advection, mixing, and pressure gradient on staggered Arakawa-C grids (Arakawa and Lamb 1977) in horizontal curvilinear coordinates and a generalized terrain-following vertical coordinate with enhanced vertical resolution near the sea surface or bottom (Marchesiello et al. 2003). Using split-explicit time-stepping, ROMS separates barotropic (depth-averaged) and baroclinic (the residual) modes with external and internal time steps and uses a generalized forward-backward algorithm for the barotropic modes and a modified predictor-corrector algorithm with forward-backward feedback for the baroclinic modes. This techinique caters both computation stability and numerical accuracy (Shchepetkin and McWilliams 2008). For advection, ROMS uses a third-order upstream-biased scheme in the horizontal and a fourth-order centered scheme in the vertical. Vertical mixing in the surface boundary layers and in the ocean interior is addressed by a non-local K-profile parameterization (KPP) scheme (Large et al. 1994) with good performance in penetrating well from the surface boundary layers into a stable thermocline in convective and wind-driven cases and producing realistic exchanges of properties between the mixed layer and thermocline when comparing with observations. The pressure gradient force is computed by a high-order, density-Jacobian algorithm which results in very accurate hydrostatic balance and retains the accuracy with nonuniform vertical grids at relatively coarse resolution (Shchepetkin and McWilliams 2003). The open lateral boundaries in the ROMS is addressed by using an adaptive algorithm which combines an outward radiation condition and a flow-adaptive nudging toward prescribed external condition and deals with outward and inward flow separately (Marchesiello et al. 2001).

The model has both idealized and realistic configurations, which are distinct in the treatment of bathymetry. We initially use the idealized version as Capet et al. (2008a) over the central California coast. This version of ROMS has been tested by Capet et al. (2008a,b,c) and their results showed that it can simulate many unique features observed in the California Current system, such as coastal upwelling, mesoscale eddies and surface mesoscale frontal

behavior.

For our study, the model domain extends from 31.6^{o}N to 40.4^{o}N in the latitude and from 120.3^{o}W to 131.1^{o}W in the longitude (see shaded region in Fig. 1(a)). In the idealized configuration, the model coastline is straight and the ocean bottom is flat with uniform depth of 3500 m. The resolution is about 7 km in the horizontal and 40 uneven grid levels in the vertical with more levels in the upper ocean (about 15 levels above 50-m depth) and fewer levels in the lower ocean (see Fig. 1(b)). The open-ocean boundary is provided by a ROMS run with the same topography, coastline and surface forcings, but a coarser resolution over a larger domain. The atmospheric forcing (momentum, freshwater and heat fluxes) is constantly given by Comprehensive Ocean-Atmosphere Dataset (COADS) climatological fields for July. The model outputs ocean current (u cross-shore, v along-shore), potential temperature (T) and salinity (S), and sea surface height (η) every six hours.

2.2. DA Method - LETKF

Data assimilation is a procedure that optimally combines information from a prior short-range forecast (i.e. background) and recent observations to estimate current state (i.e. analysis) based on forecast and observation error statistics. Following the notation conventions suggested by Ide et al. (1997), the model state is usually indicated by a vector $\mathbf{x} \in \mathbb{R}^N$ and a superscript b (a) on it denotes background (analysis) state. For the ROMS, the state vector $\mathbf{x}$ is composed of ocean current (u cross-shore, v along-shore), potential temperature (T) and salinity (S), and sea surface height (η). The observation vector is denoted by $\mathbf{y}^o \in \mathbb{R}^L$.

In this project, the local ensemble transform Kalman filter (LETKF) (Hunt et al. 2007) is chosen for the DA system to estimate the analysis state $\mathbf{x}^a$. The notation used in the LETKF is described in Table 1. From a variational point of view, the analysis mean $\bar{\mathbf{x}}^a$ is generated by minimizing the Kalman filter cost function:

$$J(\mathbf{x}) = (\mathbf{x} - \bar{\mathbf{x}}^b)^{\mathsf{T}}(\mathbf{P}^b)^{-1}(\mathbf{x} - \bar{\mathbf{x}}^b) + [\mathbf{y}^o - h(\mathbf{x})]^{\mathsf{T}}\mathbf{R}^{-1}[\mathbf{y}^o - h(\mathbf{x})] \tag{1}$$

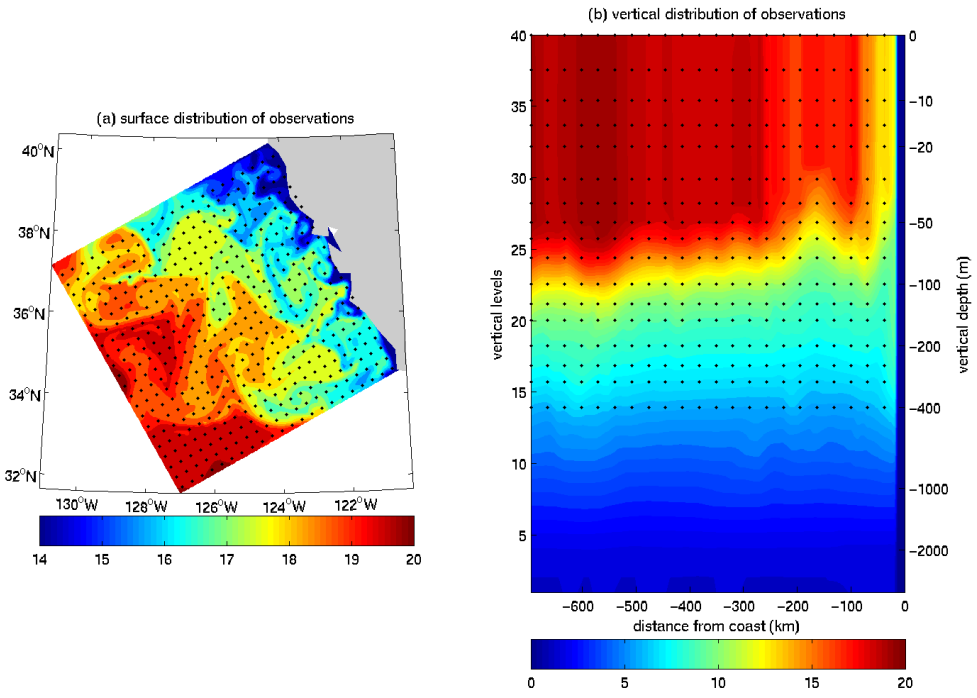

FIG. 1 Horizontal (a) and vertical (b) distribution of observing networking assimilated in the ROMS-LETKF. Shaded field is nature temperature.

where $\bar{\mathbf{x}}^b \in \mathbb{R}^N$ stands for the background ensemble mean, $\mathbf{P}^b \in \mathbb{R}^{N\times N}$ the background error covariance in ensemble space computed from background ensemble perturbations $\mathbf{X}^b \in \mathbb{R}^{N\times K}$: $\mathbf{P}^b = \frac{1}{K-1}\mathbf{X}^b(\mathbf{X}^b)^{\mathsf{T}}$, h the nonlinear observation operator, and $\mathbf{R} \in \mathbb{R}^{L\times L}$ observation error covariance. The LETKF minimizes the Kalman filter cost function that is constructed in the ensemble space through the transformation $\mathbf{x} = \bar{\mathbf{x}}^b + \mathbf{X}^b\mathbf{w}$:

$$\tilde{J}^*(\mathbf{w}) = (K-1)\mathbf{w}^{\mathsf{T}}\mathbf{w} + [\mathbf{y}^o - \bar{\mathbf{y}}^b - \mathbf{Y}^b\mathbf{w}]^{\mathsf{T}}\mathbf{R}^{-1}[\mathbf{y}^o - \bar{\mathbf{y}}^b - \mathbf{Y}^b\mathbf{w}] \tag{2}$$

where $\mathbf{w} \in \mathbb{R}^K$ in ensemble space denotes a weight vector of $\mathbf{X}^b$; $\bar{\mathbf{y}}^b \approx \mathbf{H}(\bar{\mathbf{x}}^b) \in \mathbb{R}^L$ is background ensemble mean transformed to the observation space through $\mathbf{H}$ which is the

TABLE 1 Notation for LETKF and adaptive inflation

Variable	Description
N	number of model variables
K	ensemble member size
k	ensemble index
L	number of observations
$()^{\mathsf{T}}$	transpose of a matrix or a vector
$()_{[l]}$	a quantity defined on a local region centered at the analysis grid point l
$\mathbf{x}^{b(k)}$	background state vector of the kth ensemble member with dimension $\mathbb{R}^N$
$\bar{\mathbf{x}}^b$	background ensemble mean with dimension $\mathbb{R}^N$
$\mathbf{X}^b$	background perturbation from ensemble mean with dimension $\mathbb{R}^{N\times K}$
$\mathbf{P}^b$	background error covariance matrix with dimension $\mathbb{R}^{N\times N}$
h	nonlinear observation operator projecting the background $\mathbf{x}^b$ to the observation space
$\mathbf{H}$	linear tangent matrix of h with dimension $\mathbb{R}^{L\times N}$
$\mathbf{y}^o$	observations with dimension $\mathbb{R}^L$
$\mathbf{R}$	observation covariance matrix with dimension $\mathbb{R}^{L\times L}$
$\mathbf{x}^{a(k)}$	analysis state vector of the kth ensemble member with dimension $\mathbb{R}^N$
$\bar{\mathbf{x}}^a$	analysis ensemble mean with dimension $\mathbb{R}^N$
$\mathbf{X}^a$	analysis perturbation from ensemble mean with dimension $\mathbb{R}^{N\times K}$
α	inflation factor
$\mathbf{I}$	identity matrix

tangent linear form of h; $\mathbf{Y}^b \approx \mathbf{H}(\mathbf{X}^b) \in \mathbb{R}^{L\times K}$ is background ensemble perturbation in the observation space.

In the $\mathbf{w}$ coordinate, the background mean $\bar{\mathbf{w}}^b = 0$ and background error covariance $\tilde{\mathbf{P}}^b = (K-1)^{-1}\mathbf{I}$. The solution of minimizing the cost function in ensemble space is the analysis weight vector $\bar{\mathbf{w}}^a$:

$$\tilde{\mathbf{P}}^a = [(K-1)\mathbf{I} + (\mathbf{Y}^b)^{\mathsf{T}}\mathbf{R}^{-1}(\mathbf{Y}^b)]^{-1} \tag{3}$$

$$\bar{\mathbf{w}}^a = \tilde{\mathbf{P}}^a(\mathbf{Y}^b)^{\mathsf{T}}\mathbf{R}^{-1}(\mathbf{y}^o - \bar{\mathbf{y}}^b) \tag{4}$$

where $\tilde{\mathbf{P}}^a \in \mathbb{R}^{K\times K}$ is analysis error covariance matrix in the ensemble space. The analysis spread is a combination of background spread weighted by $\mathbf{W}^a = [(K-1)\tilde{\mathbf{P}}^a]^{1/2}$.

The LETKF computes the analysis at each grid point. In addition, in order to reduce

the effect of rank deficiency, the LETKF assimilates observations within a certain distance from each grid point and $\mathbf{R}^{-1}$ is thus substituted with $\mathbf{R}_{[l]}^{-1}$, where the subscript $[l]$ stands for the quantity defined on a local area centered at the analysis grid point l. Hence, $\bar{\mathbf{w}}^a$, $\tilde{\mathbf{P}}^a$ and $\mathbf{W}^a$ are actually performed in local areas. Moreover, to avoid underestimating the error covariance, the LETKF inflates background perturbations by dividing by the inflation parameter α in the first term of $\tilde{\mathbf{P}}^a$. α could be either a constant for all model grid points or varying locally where α is replaced by $\alpha_{[l]}$ (see Section 3.1.1 for details). Besides, the LETKF could be extended to 4D-LETKF which assimilates observations $\mathbf{y}^o$ not only collected at the analysis time. Assuming there are totally t_n observations in an analysis cycle, therefore, when assimilating asynchronous observations in local areas and applying inflation, $\tilde{\mathbf{P}}^a$, $\bar{\mathbf{w}}^a$ and $\mathbf{W}^a$ are

$$\tilde{\mathbf{P}}_{[l]}^a = \left[\frac{(K-1)}{\alpha}\mathbf{I} + \sum_{\tau_j=1}^{\tau_j=t_n} (\mathbf{Y}_{[l]}^b(\tau_j))^{\mathsf{T}} \mathbf{R}_{[l]}^{-1}(\tau_j)(\mathbf{Y}_{[l]}^b(\tau_j))\right]^{-1} \tag{5}$$

$$\bar{\mathbf{w}}_{[l]}^a = \tilde{\mathbf{P}}_{[l]}^a \left\{ \sum_{\tau_j=1}^{\tau_j=t_n} (\mathbf{Y}_{[l]}^b(\tau_j))^{\mathsf{T}} \mathbf{R}_{[l]}^{-1}(\tau_j)[\mathbf{y}_{[l]}^o(\tau_j) - \bar{\mathbf{y}}_{[l]}^b(\tau_j)] \right\} \tag{6}$$

$$\mathbf{W}_{[l]}^a = [(K-1)\tilde{\mathbf{P}}_{[l]}^a]^{1/2} \tag{7}$$

where τ_j represents the time within an analysis cycle, $\tau_j = 1$ is the first observation right after the previous analysis cycle and $\tau_j = t_n$ is the last observation within the current analysis cycle.

The analysis ensemble mean $\bar{\mathbf{x}}^a$ and perturbation $\mathbf{X}^a$ are calculated locally.

$$\bar{\mathbf{x}}_{[l]}^a = \bar{\mathbf{x}}_{[l]}^b + \mathbf{X}_{[l]}^b \bar{\mathbf{w}}_{[l]}^a \tag{8}$$

$$\mathbf{X}_{[l]}^a = \mathbf{X}_{[l]}^b \mathbf{W}_{[l]}^a \tag{9}$$

The analysis state vector of the kth ensemble member is obtained in model space by

$$\mathbf{x}^{a(k)} = \bar{\mathbf{x}}^a + \mathbf{X}^{a(k)} \tag{10}$$

Therefore, apart from estimating the time-evolving background error covariance including flow-dependent information, the LETKF has several other advantages. Firstly, the analysis could be calculated locally at each model grid point using surrounding observations. This ameliorates the problem of rank deficiency due to finite ensemble size. Secondly, performing the analysis cycle at each grid point allows the implementation of efficient parallel computation. Thirdly, the portable algorithm could be easily coupled with other techniques, such as localization (see Section 1.2.1 for details), inflation (see Section 3.1.1 for details) and/or asynchronous observations, to improve analysis accuracy (Hunt et al. 2007).

3. Results

3.1. Experiments with ROMS-LETKF

Miyoshi et al. (2010) has coupled the LETKF with the idealized-configured ROMS (named as ROMS-LETKF). All experiments that have been done so far are based on this ROMS-LETKF system. The ROMS-LETKF operates localization techniques on the inverse observation error covariance in both horizontal and vertical directions. Basic parameters used in the ROMS-LETKF are listed in Table 2.

TABLE 2 LETKF parameters

Parameters	Corresponding Value
Ensemble size	20
Horizontal localization scale	5 grids (i.e. 35 km)
Vertical localization scale	50 m

The identical twin OSSEs are conducted under the perfect model assumption. The nature run (considered as truth) is obtained by running the ROMS itself for almost one year after spinning up for about four years. Synthetic observations are then generated from the nature run by adding Gaussian random error to the true state. The observation error standard deviations of each variables are given in Table 3. The variables are observed in a relatively

realistic observing network (see Fig. 1): the current (u, v) and sea surface height (η) are only observed every 5 grid points at surface as orthogonally mapping HF radar velocity and satellite observations, and potential temperature (T) and salinity (S) are observed vertically in 17 layers from surface to 400 m beneath as glider observations. No observations are available in deep ocean.

TABLE 3 Standard deviation of observation errors for assimilated variables

Observation Type	u	v	T	S	η
Standard Deviation of Error	0.1m/s	0.1 m/s	1 K	0.1 psu	0.03 m

The 20 ensemble members in the ROMS-LETKF are randomly picked from the four-year spin up period of the nature run at initial time. The lateral boundary conditions and the atmospheric forcing for the 20 members are the same as those for the nature run. Observations are assimilated every six hours. All experiments are integrated for two months.

3.1.1) Parameters for Adaptive Inflation

Localization and inflation are two essential aspects to improve analysis accuracy in an EnKF method. We firstly concentrate on two issues in the LETKF, inflation and localization, which are discussed as follows.

Inflation is a technique that expands the ensemble perturbations to avoid underestimating the error covariance. It can be implemented through (i) simply multiplying background ensemble perturbations by a factor slightly larger than 1, i.e. multiplicative inflation (Anderson and Anderson 1999; Hamill et al. 2001) ; (ii) adding a small random perturbation to background ensemble spread, i.e. additive inflation (Ott et al. 2004; Whitaker et al. 2008; Houtekamer et al. 2009); (iii) linearly combined background and analysis ensemble perturbations, i.e. relaxation-to-prior method (Zhang et al. 2004); or (iv) adaptively estimating multiplicative inflation parameters. i.e. adaptive inflation (Anderson 2007, 2009; Li et al. 2009; Miyoshi 2011). The former three methods are required manually tuning their

parameters, while the adaptive inflation does not. The ROMS-LETKF provides several options (multiplicative, additive, and adaptive) for covariance inflation. We apply the adaptive inflation in our experiments.

In the adaptive inflation of the ROMS-LETKF, the inflation parameter α is updated by the innovation statistics at each grid point and each data assimilation interval based on the Gaussian assumption (Miyoshi 2011) and thus we use $\alpha_{[l]}$ here instead. The initial value of background inflation parameter $\bar{\alpha}^b_{[l]}$ and its variance $\nu^b_{[l]}$ are prescribed to update the inflation parameter and need to be manually tunned.

3.1.2) Observation Influence and Inflation Impacts

The observations are usually concentrated in the upper ocean. In our experiments, if not specifically mentioned, T and S observations are only down to 400 m beneath and there are no observations below 400 m (see Fig. 1(b)). In the current version of the ROMS-LETKF, the vertical localization scaling is constantly set as 50 m. Assuming the Gaussian distribution of the observation influence, this implies that the observation influence ends around 580 m beneath if the deepest observation is made at 400 m below the surface. In the experiment using adaptive inflation with 1% initial inflation (i.e. Exp_adpinfl.v1 in Table 4), the vertical profiles of the analysis RMSEs and ensemble spreads averaged on the whole model domain have a significant peak around level 12 ($\approx$ -544 m) (see the blue lines in Fig. 2). These peaks in the vertical analysis RMSEs and spreads are shown to move up or down if the observations are made shallower or deeper. Hence, the peak in the vertical analysis RMSEs is thought as the results from the termination of observation influence and the implementation of 1% inflation in the deep ocean.

This kind of peaks can be dramatically reduced in two ways. One is simply setting the initial inflation to zero in the adaptive inflation (i.e. Exp_adpinfl.v2 in Table 4) and the other is manually adjusting the inflation gradually to zero at the level where the observation influence terminates (i.e. Exp_adpinfl.v3 in Table 4). Both ways suggest no inflation for no

TABLE 4 Experiments design

Experiments	Adaptive inflation	Adaptive inflation	Adaptive + manually adjusted inflation
	Exp_adpinfl.v1	Exp_adpinfl.v2	Exp_adpinfl.v3
Inflation Parameters	1% at initial;	0% at initial;	1% at initial; If inflation, $\bar{\alpha}^b_{[l]}$ decrease to $10\%\bar{\alpha}^b_{[l]}$ level 13, to $5\%\bar{\alpha}^b_{[l]}$ at level 12; 0 inflation below level 12

observations. Based on our two-month primary tests (see Table 4 for experiments design), the two ways show same ability to reduce the peak in the vertical analysis spreads (see Fig. 2).

3.1.3) Extension to 4DLETKF

The extension to 4DLETKF is also tested in the OSSE framework to assimilate asynchronous observations taken at intermediate times during an analysis cycle. The 4DLETKF OSSE is initially conducted to assimilate a single surface temperature observation at the beginning of a 24-hr assimilation window. The evolution of the analysis increment during the 24-hr analysis cycle is shown on Fig. 3.

On Fig. 3 (a)-(c), the analysis increment evolves and moves along the background flow through the entire cycle even the observation is assimilated at the beginning. The movement of the center of the analysis increment during the assimilation window is clearly observed on Fig. 3(d). Hence, 4DLETKF is capable to capture the evolution of the increments within an analysis cycle.

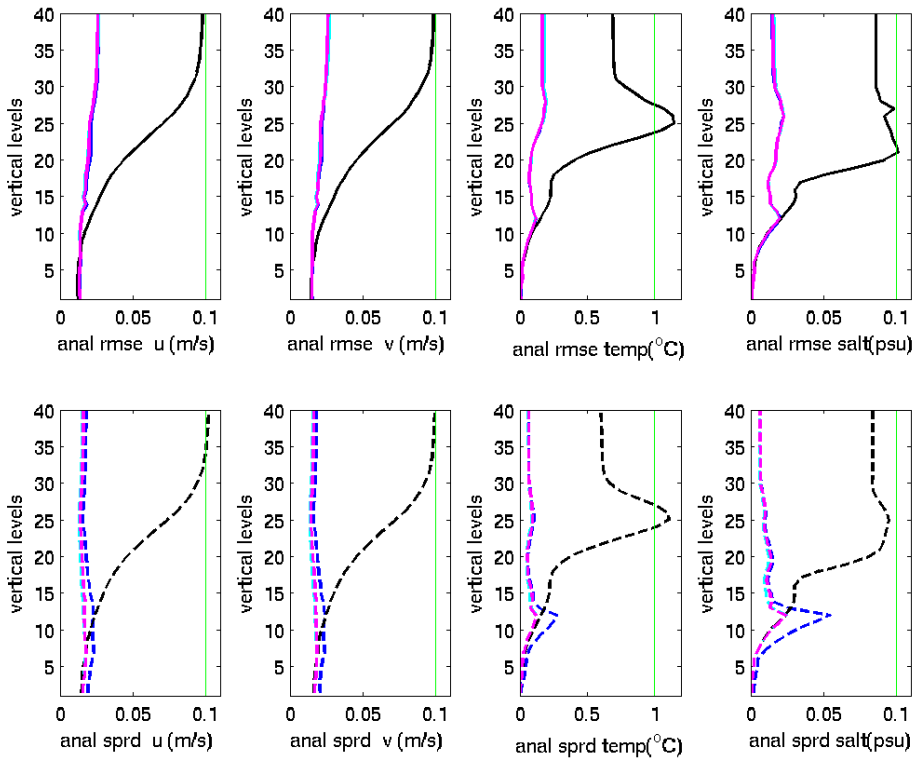

FIG. 2 Vertical profile of analysis RMSEs (upper) and spread (bottom) averaged in the entire model domain and the last month for four 3D variables in the Exp_adpinfl.v1 (blue), Exp_adpinfl.v2 (cyan), Exp_adpinfl.v3 (pink) and Exp_Noobs (black) (Exp_Noobs is the experiments without assimilating observations). The green solid lines indicate standard deviation of the corresponding observation errors.

3.2. Step-wise linear vertical localization for stratification

The current LETKF applies a Gaussian distance-dependent function to the inverse observation error covariance $\mathbf{R}^{-1}$ in both horizontal and vertical directions to remove the spurious impact of the observations far away from the analysis grid point. The vertical localization scale is set as a constant, 50m. Using constant vertical localization scale in the upper ocean allows the surface observations to impact the upper 180m in the vertical. Most of the obser-

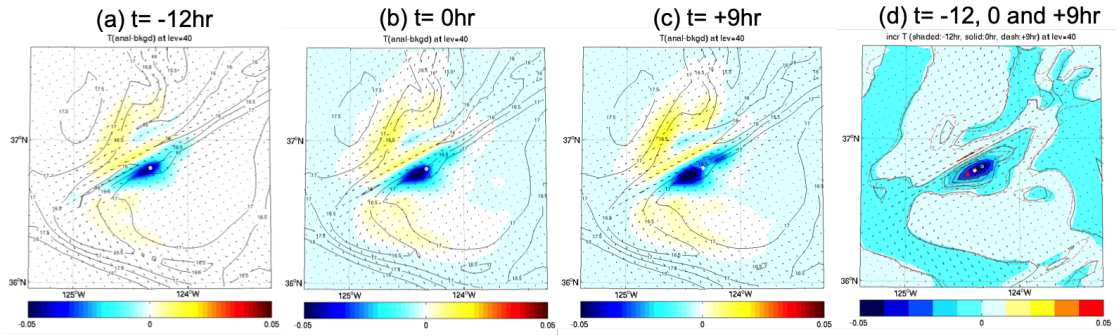

FIG. 3 Temperature analysis increments at the surface of a 4DLETKF experiment assimilating a single sea surface temperature observation at the beginning of the 24-hr assimilation window. T increment (shaded) and background (contours) at (a) the beginning of an analysis cycle (t = -12hr), (b) the middle of the analysis cycle (t = 0hr), and (c) the end of the analysis cycle (t = +9hr); The white dots on (a),(b), and (c) indicate the location of the single T observation. (d) the movement of T increments during the analysis cycle. The cyan, white, and red dots on (d) are the center of analysis increment at t= -12 hr, 0hr and +9hr, respectively.

vations concentrate at the surface, hence the constant vertical localization scale works well in the model level 40-26. Due to the dramatical decrease in the number of observation beneath the surface and the increase in the depth among the model vertical levels, the constant vertical localization could not handle this situation very well. Hence, the manually setup step-wise linear vertical localization is proposed initially to test their impacts on the LETKF performance before applying dynamically-varying vertical localization into the LETKF.

Two types of step-wise linear vertical localization scale are designed as shown in Fig. 4. The LETKF using both step-wise linear vertical localization scales assimilates surface observations in the top 180m (model level 40-19), as the LETKF using constant vertical localization scale does. Between 200m and 1000m (level 18- 8), the LETKF using both step-wise linear vertical localization scales assimilates some amount of observations, and

the number of assimilated observation decreases as the model depth increases; whereas the LETKF using constant vertical localization scales cuts off the observation influence below the depth of 600m. Below the depth of 1200m (model level 7-1), the LETKF with vertical localization scale in Fig.4(a) does not assimilate any observations, while the LETKF with vertical localization scale in Fig. 4(b) still assimilates the observation at 400m.

The impacts of step-wise linear vertical localization scale are examined by comparing with the LETKF experiments using constant vertical localization scale and infinite vertical localization scale in which all the observation are assimilated in every model level, i.e. no vertical localization is used. The inflation scheme is the same as in Exp_adpinfl.v2 in Table 4.

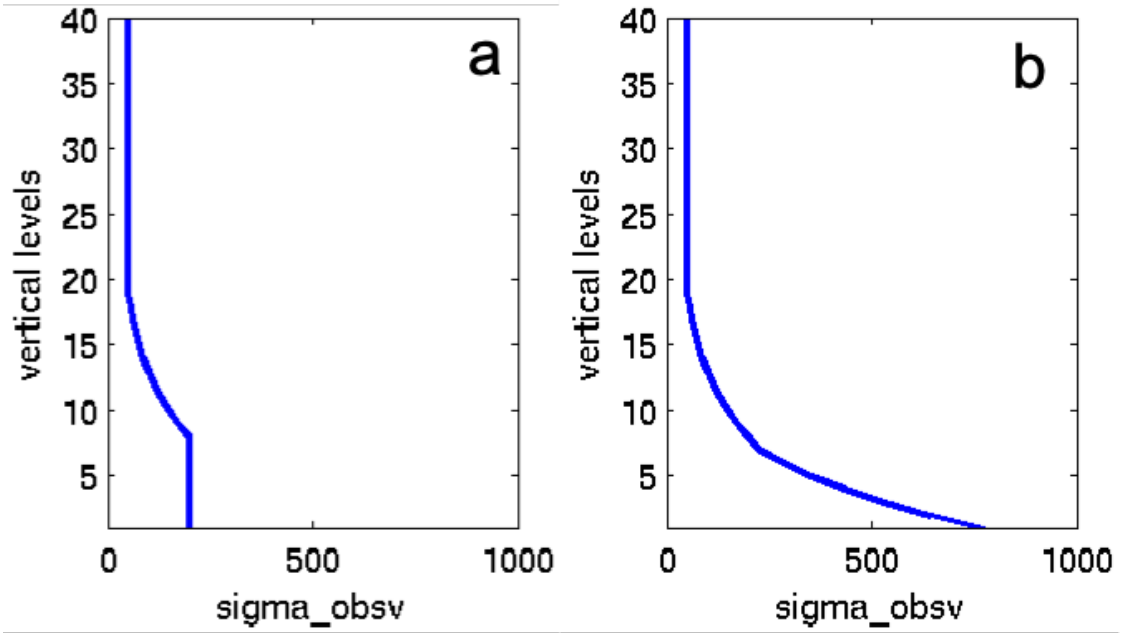

FIG. 4 Step-wise linear vertical localization scale. (a) σ_{obsv}=50m for the model level 19-40, and 200m for the model level 7-1, and linearly increasing from 50m to 200m between the model level 8-18; (b) σ_{obsv}=50m for the model level 19-40, linearly increasing from 50m to 200m between the model level 8-18, and then linearly increasing down to the ocean bottom.

On Fig. 5, the analysis rmse of u, v, T and S is smaller in the experiments using step-

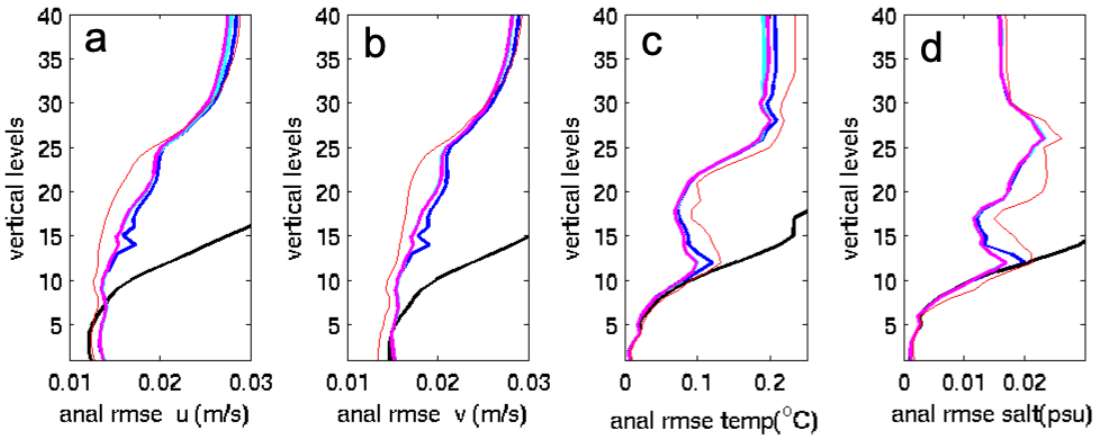

FIG. 5 Vertical profile of analysis rmse averaged over the entire model domain and the last month for (a)u, (b) v, (c) T, and (d) S. Blue is for the constant vertical localization scale, cyan for the step-wise linear vertical localization scale in Fig.4(a), pink for the step-wise linear vertical localization scale in Fig. 4(b), orange for no vertical localization used and black for no observation is assimilated.

wise linear vertical localization length scale than the ones using constant vertical localization scale, especially in the upper 400m (around the model level 40 -12). The difference in the LETKF performance between the two types of step-wise linear vertical localization scales is subtle. Compared with the LETKF with no use of vertical localization, i.e. assimilating all observations at every model level, the LETKF with step-wise linear vertical localization has better performance for temperature and salinity in the entire vertical column, but not for currents beneath 180m.

3.3. Dynamic Constraints

Dynamic constraints in the LETKF could be realized with the help of the variable localization (Kang et al. 2011) which zeros out the corresponding parts in background error covariance between the uncorrelated variables. In our work, we would like to use two sets of

control variables for dynamic constraints.

Two main dynamic balances, hydrostatic and geostrophic balances, are considered in the LETKF. The hydrostatic static balance is

$$\frac{\partial p}{\partial z} = -(\rho_0 + \rho)g \tag{11}$$

where p is seawater pressure, g gravitational acceleration, ρ_0 the Boussinesq approximation of the seawater mean density and ρ seawater density anomaly. The geostrophic balance is

$$u_g = -\frac{g}{f}\frac{\partial \eta}{\partial y} \tag{12}$$

$$v_g = \frac{g}{f}\frac{\partial \eta}{\partial x} \tag{13}$$

where f is Coriolis parameter and η sea surface height.

According to the unique features in the coastal ocean, we combine the basic strategies of Weaver et al. (2005) and Li et al. (2008): (i) Temperature T and salinity S are used to separate other model state variables into balanced and unbalanced parts based on underlying hydrostatic and geostrophic balances; (ii) A new control vector is created by original T and S but unbalanced part of η, u and v; (iii) This new control vector is used in the LETKF incorporated with variable localization (Kang et al. 2011) to generate ensemble analysis.

Similar to the formulation in Li et al. (2008), the dynamic balances are applied in to decompose the sea surface height η to steric and nonsteric components and u/v to geostrophic and ageostrophic parts:

$$\mathbf{x}_{\eta} = \mathbf{\Pi}\mathbf{x}_{TS} + \mathbf{x}_{\eta'} \tag{14}$$

$$\mathbf{x}_{uv} = \mathbf{\Gamma}_{TS}\mathbf{x}_{TS} + \mathbf{\Gamma}_{\eta'}\mathbf{x}_{\eta'} + \mathbf{x}_{u''v''} \tag{15}$$

where $\mathbf{x}_{\eta'}$ is nonsteric sea surface height, $\mathbf{x}_{u''v''}$ is ageostrophic u/v.

Hence, the background state vector and the new control vector become:

$$\mathbf{x}^b = \boldsymbol{\mathcal{F}}\mathbf{x}^b_{\mathsf{new}} = \begin{pmatrix} \mathbf{1} & \mathbf{0} & \mathbf{0} \\ \boldsymbol{\Pi} & \mathbf{1} & \mathbf{0} \\ \boldsymbol{\Gamma}_{TS} & \boldsymbol{\Gamma}_{\eta'} & \mathbf{1} \end{pmatrix} \begin{pmatrix} \mathbf{x}_{TS} \\ \mathbf{x}_{\eta'} \\ \mathbf{x}_{u''v''} \end{pmatrix} \tag{16}$$

$$\mathbf{x}^{\mathsf{T}}_{\mathsf{new}} = (\mathbf{x}^{\mathsf{T}}_{TS}, \mathbf{x}^{\mathsf{T}}_{\eta'}, \mathbf{x}^{\mathsf{T}}_{u''v''}) \tag{17}$$

where $\boldsymbol{\mathcal{F}}$ is transformation matrix.

Then variable localization is applied to transform the new background ensemble perturbation and the new cost function in ensemble space becomes:

$$\mathbf{x}_{\mathsf{new}} - \mathbf{x}^b_{\mathsf{new}} = \mathbf{X}^b_{\mathsf{new}}\mathbf{w}_{\mathsf{new}} = \begin{pmatrix} \mathbf{X}^b_{TS} & \mathbf{0} & \mathbf{0} \\ \mathbf{0} & \mathbf{X}^b_{\eta'} & \mathbf{0} \\ \mathbf{0} & \mathbf{0} & \mathbf{X}^b_{u''v''} \end{pmatrix} \begin{pmatrix} \mathbf{w}_{TS} \\ \mathbf{w}_{\eta'} \\ \mathbf{w}_{u''v''} \end{pmatrix} \tag{18}$$

$$\tilde{J}^*(\mathbf{w}_{\mathsf{new}}) = (K-1)\mathbf{w}^{\mathsf{T}}_{\mathsf{new}}\mathbf{w}_{\mathsf{new}} + (\mathbf{d} - \mathbf{H}\boldsymbol{\mathcal{F}}\mathbf{X}^b_{\mathsf{new}}\mathbf{w}_{\mathsf{new}})^{\mathsf{T}}\mathbf{R}^{-1}(\mathbf{d} - \mathbf{H}\boldsymbol{\mathcal{F}}\mathbf{X}^b_{\mathsf{new}}\mathbf{w}_{\mathsf{new}}) \tag{19}$$

where the innovation $\mathbf{d}$ and observation error covariance $\mathbf{R}$ do not change. The solution of minimizing the new cost function is

$$\bar{\mathbf{w}}^a_{\mathsf{new}} = \tilde{\mathbf{P}}^a_{\mathsf{new}}(\mathbf{H}\boldsymbol{\mathcal{F}}\mathbf{X}^b_{\mathsf{new}})^{\mathsf{T}}\mathbf{R}^{-1}\mathbf{d} \tag{20}$$

$$\tilde{\mathbf{P}}^a_{\mathsf{new}} = [(K-1)\mathbf{I} + (\mathbf{H}\boldsymbol{\mathcal{F}}\mathbf{X}^b_{\mathsf{new}})^{\mathsf{T}}\mathbf{R}^{-1}(\mathbf{H}\boldsymbol{\mathcal{F}}\mathbf{X}^b_{\mathsf{new}})]^{-1} \tag{21}$$

$$\tag{22}$$

The transformation matrix $\boldsymbol{\mathcal{F}}$ is used to transform the new analysis increment back to the original:

$$\Delta\bar{\mathbf{x}}^a = \boldsymbol{\mathcal{F}}\delta\bar{\mathbf{x}}^a_{\mathsf{new}} = \boldsymbol{\mathcal{F}}\mathbf{X}^b_{\mathsf{new}}\bar{\mathbf{w}}^a_{\mathsf{new}} = \begin{pmatrix} \mathbf{X}^b_{TS}\bar{\mathbf{w}}^a_{TS} \\ \boldsymbol{\Pi}\mathbf{X}^b_{TS}\bar{\mathbf{w}}^a_{TS} + \mathbf{X}^b_{\eta'}\bar{\mathbf{w}}^a_{\eta'} \\ \boldsymbol{\Gamma}_{TS}\mathbf{X}^b_{TS}\bar{\mathbf{w}}^a_{TS} + \boldsymbol{\Gamma}_{\eta'}\mathbf{X}^b_{\eta'}\bar{\mathbf{w}}^a_{\eta'} + \mathbf{X}^b_{u''v''}\bar{\mathbf{w}}^a_{u''v''} \end{pmatrix} \tag{23}$$

Single observation experiments with/without dynamic constraints and variable localization are done to primarily test the impact of dynamic constraints in the 3DLETKF framework. The vertical structure of the LETKF analysis increments of experiments assimilating

single sea surface height are shown on Fig. 6. Constant vertical localization is applied in both single observation experiments.

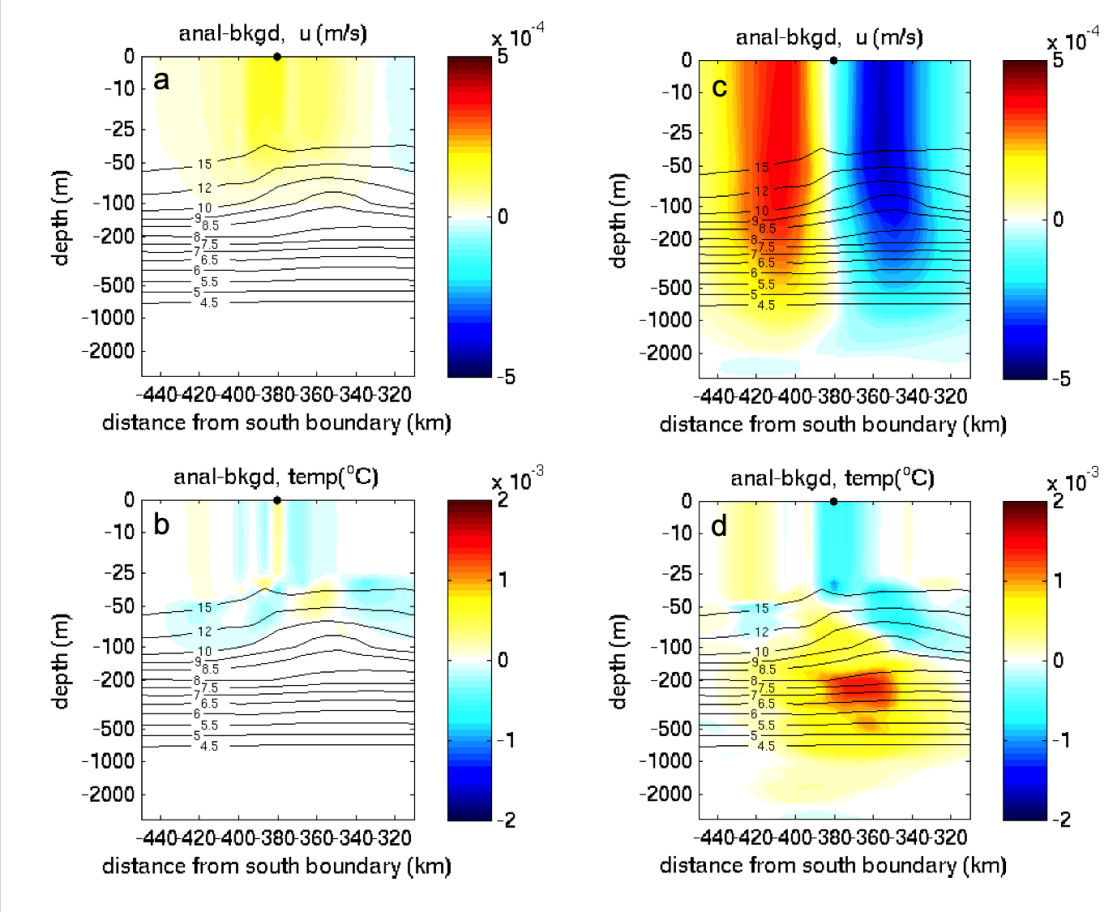

FIG. 6 Vertical cross section of analysis increments of u (upper) and temperature (bottom) of the single sea surface height observation experiments with and without dynamic constraint. Black dot at the surface level indicates the location of the single sea surface height observation. (a) u increment in LETKF without constraint; (b) T increment in LETKF without constraint; (c) u increment in LETKF with constraint; (d) T increment in LETKF with constraint

Due to the vertical localization with constant vertical localization scale, u and T on Fig. 6(a) and (b) are updated within the vertical localization influence radius in the LETKF experiment. After applying dynamic constraint and variable localization, u and T on Fig.6(c)

and (d) are updated even outside the vertical localization radius. This is because the steric η is due to the thermal expansion of the whole sea water column. Through the dynamic constraints and variable localization in the LETKF, the increment in the steric η is passed to T and S in the whole column even the vertical localization is applied.

4. Concluding Remarks

4.1. Summary

The LETKF coupled with a regional coastal ocean model (ROMS) is used in this project to study the stratification and dynamic constraints of the coastal ocean in the data assimilation under the OSSEs framework along the Central California coastal area.

The primary results show that the LETKF works well to assimilate remote and in-situ observations along the Central California coastal area. Due to the lack of observation in the deep ocean, the inflation in the LETKF should be turned off outside the observation influence radius to avoid large error near the edge of observation influence radius. The extension of LETKF to 4DLETKF can assimilate the asynchronous observations and is capable to capture the evolution of the increments within an analysis cycle. The LETKF using the step-wise linear vertical localization scale gives smaller analysis rmse of u, v, T and S compared with the constant vertical localization scale, especially in the upper 400m where in-situ observations are collected. Based on the results of single observation experiments, using the LETKF with dynamic constraints and variable localization, the increment in steric η can be passed to T and S in the whole vertical column even the vertical localization is applied.

4.2. Potential Development

Potential development related to the aspects in the introduction are as follows:

4.2.1) Stratification

As the primary results we showed, the constant vertical localization scales works quite well in the upper ocean where dense observations are available. In the deep ocean with sparse or even no observations, the analysis RMSEs are not as good as we expected. Besides the difference in the observation density between the upper and deep ocean, the oceanic motion in different layers has different scales. Testing of manually setup step-wise linear vertical localization length could improve the LETKF performance to some extent, it would be more reasonable to use the vertical localization scale dynamically associated with the vertical stratification of the ocean in order to grasp more information from observations. First, the depths of each ocean layers can be determined. For example, the mixed layer depth (MLD) could be calculated based on an optimal definition proposed by Kara et al. (2000). Then, we could use a small scale in the mixed layer, a large scale in the deep ocean and a transition between the two scales in thermocline. Within the mixed layer and the deep ocean, the scales could be set as constants. Based on Miyoshi and Kunii (2012), the slope of the transition between small and larger localization scales matters. a dynamically-varying transition in the vertical localization scales could be configured near the edge between two layers and also within the thermocline, vertically uneven scales with smaller scale above the edge and larger scale below the edge (Personal conversation with Dr. T. Miyoshi). In the meantime, the adaptive inflation in experiments using vertically-varying localization scales also needs to be paid attention to.

4.2.2) Dynamic Constraints

The impact of dynamic constraint is initially examined in the single observation experiments. The further investigation can be done through the comparison between full observation experiments.

In the single observation experiments, we used ageostrophic currents to construct new

state vector in the LETKF with dynamic constraint. An alternative option of constructing new state vector is using ageostrophic streamfunction and velocity potential, rather than ageostrophic currents based on the following relationship:

$$u = -\frac{\partial \psi}{\partial y} + \frac{\partial \chi}{\partial x} \tag{24}$$

$$v = \frac{\partial \psi}{\partial x} + \frac{\partial \chi}{\partial y} \tag{25}$$

The reason of using streamfunction and velocity potential instead of horizontal velocity components is homogeneous and isotropic self-error covariance of ageostrophic streamfunction and velocity potential and zero cross-error covariance of them.

The experiments with dynamic constraints using streamfunction and velocity potential can also be conducted and compared with these using horizontal velocity components and these without constraints.

4.2.3) Multiscale LETKF

The multiscale method introduced by Li et al. (2012) can be employed in the LETKF scheme to address multiscale dynamics and observations following the similar steps as Li et al. (2012). (i) Background state vector $\mathbf{x}^b$ is divided large (denoted by subscript L) and small (denoted by subscript S) scale components, namely $\mathbf{x}^b = \mathbf{x}^b_{\mathsf{L}} + \mathbf{x}^b_{\mathsf{S}}$, by using an appropriate spatial filter. Due to the complex coastline geometry in the coastal area, a Gaussian horizontal smoothing function, instead of trigonometric functions, is used to separate large and small scale components. The smoothing length scale in the Gaussian smoothing function is dynamically determined from the Rossby deformation radius. (ii) In the meantime, the observations $\mathbf{y}^o$ are also categorized into dense (denoted by superscript d) and coarse (denoted by superscript c) observations in space, $\mathbf{y}^{o\mathsf{d}}$ and $\mathbf{y}^{o\mathsf{c}}$, based on the density of observing networks and an assumption that the errors of $\mathbf{y}^{o\mathsf{d}}$ and $\mathbf{y}^{o\mathsf{c}}$ are uncorrelated are made. The dense observations $\mathbf{y}^{o\mathsf{d}}$ could be partitioned into large and small parts using the spatial filter: $\mathbf{y}^{o\mathsf{d}} = \mathbf{y}^{o\mathsf{d}}_{\mathsf{L}} + \mathbf{y}^{o\mathsf{d}}_{\mathsf{S}}$, while the coarse observations $\mathbf{y}^{o\mathsf{c}}$ only contain large-scale information and

could not be partitioned. $\mathbf{R}_{\mathsf{L}}^{\mathsf{d}}$, $\mathbf{R}_{\mathsf{S}}^{\mathsf{d}}$ and $\mathbf{R}^{\mathsf{c}}$ are corresponding error covariances of $\mathbf{y}_{\mathsf{L}}^{o\mathsf{d}}$, $\mathbf{y}_{\mathsf{S}}^{o\mathsf{d}}$ and $\mathbf{y}^{o\mathsf{c}}$. (iii) The multiscale LETKF (MS-LETKF) is be formulated by minimizing the Kalman filter cost functions of large and small-scale components which can be built in the ensemble space on the basis of the Multiscale-3Dvar formulation in Li et al. (2012). Details for the MS-LETKF formulation are shown in the Appendix A. (iv) Dynamic constraints can also be applied in the MS-LETKF with different consideration for large- and small- scale component respectively. (v) The distance-dependent localization function, which can handle the stratification in the vertical, can be applied to the inverse of observation error covariance, $(\mathbf{R}_{\mathsf{L}}^{\mathsf{d}})^{-1}$, $(\mathbf{R}_{\mathsf{S}}^{\mathsf{d}})^{-1}$ and $(\mathbf{R}^{\mathsf{c}})^{-1}$ in the MS-LETKF. (vi) The adaptive inflation can be implemented in the MS-LETKF as well. The inflation parameters can be tuned and updated for large and small scale components separately. (vii) The comparison between the experiments using the MS-LETKF and using the LETKF can be done to test the performance of the MS-LETKF.

4.2.4) Assimilation of HF Radar Radial Velocity

So far we have done a series of OSSEs of HF radar-mapped surface velocity vector, which covers the entire model domain. The LETKF formulation and coding based on Shulman and Paduan (2009) to assimilate radial velocity.

At the beginning stage, the observing network of HF radar radial velocity can be built in the OSSE. The observation error covariance $\mathbf{R}^p$ is created for radials and substitutes for $\mathbf{R}$ in the LETKF. The observation operator h in the LETKF formulation can then be changed to h_R that interpolates background velocity vectors on model grids to the observation locations and also projects the velocity onto the direction of the corresponding radial, transforming vectors to scalars. The linear tangent matrix of h, namely $\mathbf{H}$, can be replaced by $\mathbf{H}_R$. $\mathbf{H}_R^{\mathsf{T}}$ transforms the scalars back to vectors at observation locations and interpolates the vector back to the model grid points. In the LETKF, the background perturbation in observation space is revised to $\mathbf{Y}_R^b = \mathbf{H}_R(\mathbf{X}^b)$.

5. Acknowledgement

The support of Office of Naval Research Grant N00014-09-1-0418 and N00014-10-1-055 is gratefully acknowledged. Thanks are due to Dr. Zhijin Li of NASA Jet Propulsion Laboratory/California Institute of Technology and Professor James C. McWilliams of University of California, Los Angeles for helping strengthen this work.

APPENDIX A

The Formulation of Multiscale LETKF

The multiscale LETKF (MS-LETKF) is generated by minimizing the Kalman filter cost function that is constructed in the ensemble space and it is formulated for large and small scale components respectively.

A1. Separation of Large and Small Scale Components of Background

A Gaussian horizontal smoothing function introduced by Li et al. (2012), rather than widely used trigonometric functions, is used to separate large and small scale components of background state vector in each ensemble member owing to the complex coastline geometry in the coastal area. The Rossby deformation radius is dynamically chosen as the smoothing length scale in Gaussin smoothing function. Hence, the background state vector of kth ensemble member, $\mathbf{x}^{b(k)}$, is divided into $\mathbf{x}^{b(k)} = \mathbf{x}_{\mathsf{L}}^{b(k)} + \mathbf{x}_{\mathsf{S}}^{b(k)}$. The corresponding background error covariance is denoted by $\mathbf{P}_{\mathsf{L}}^{b}$ and $\mathbf{P}_{\mathsf{S}}^{b}$.

A2. Separation of Dense and Coarse Observations

The observations $\mathbf{y}^{o}$ are separated into dense and coarse observations based on the spatial resolution of their observing networks: $\mathbf{y}^{o\mathsf{d}}$ and $\mathbf{y}^{o\mathsf{c}}$ and the errors of $\mathbf{y}^{o\mathsf{d}}$ and $\mathbf{y}^{o\mathsf{c}}$ are assumed to be uncorrelated with each other. Moreover, the dense observation contains large and small scale information which could be separated by the Gaussian smoothing function: $\mathbf{y}^{o\mathsf{d}} = \mathbf{y}_{\mathsf{L}}^{o\mathsf{d}} + \mathbf{y}_{\mathsf{S}}^{o\mathsf{d}}$, whereas the coarse observations could not be separated because they only have large scale information.

The nonlinear observation operators for dense and coarse observations are denoted as h^{d}

and h^{c} and their tangent linear forms are $\mathbf{H}^{\mathsf{d}}$ and $\mathbf{H}^{\mathsf{c}}$, respectively. Hence, the large scale background components in the dense and coarse observation space are represented by

$$h^{\mathsf{d}}(\mathbf{x}_{\mathsf{L}}^{b}) \approx \mathbf{H}^{\mathsf{d}}\bar{\mathbf{x}}_{\mathsf{L}}^{b} + \mathbf{H}^{\mathsf{d}}\mathbf{X}_{\mathsf{L}}^{b} = \bar{\mathbf{y}}_{\mathsf{L}}^{b\mathsf{d}} + \mathbf{Y}_{\mathsf{L}}^{b\mathsf{d}} \tag{A1}$$

$$h^{\mathsf{c}}(\mathbf{x}_{\mathsf{L}}^{b}) \approx \mathbf{H}^{\mathsf{c}}\bar{\mathbf{x}}_{\mathsf{L}}^{b} + \mathbf{H}^{\mathsf{c}}\mathbf{X}_{\mathsf{L}}^{b} = \bar{\mathbf{y}}_{\mathsf{L}}^{b\mathsf{c}} + \mathbf{Y}_{\mathsf{L}}^{b\mathsf{c}} \tag{A2}$$

Similarly, the small scale background component in the dense and coarse observation space are

$$h^{\mathsf{d}}(\mathbf{x}_{\mathsf{S}}^{b}) \approx \mathbf{H}^{\mathsf{d}}\bar{\mathbf{x}}_{\mathsf{S}}^{b} + \mathbf{H}^{\mathsf{d}}\mathbf{X}_{\mathsf{S}}^{b} = \bar{\mathbf{y}}_{\mathsf{S}}^{b\mathsf{d}} + \mathbf{Y}_{\mathsf{S}}^{b\mathsf{d}} \tag{A3}$$

$$h^{\mathsf{c}}(\mathbf{x}_{\mathsf{S}}^{b}) \approx \mathbf{H}^{\mathsf{c}}\bar{\mathbf{x}}_{\mathsf{S}}^{b} + \mathbf{H}^{\mathsf{c}}\mathbf{X}_{\mathsf{S}}^{b} = \bar{\mathbf{y}}_{\mathsf{S}}^{b\mathsf{c}} + \mathbf{Y}_{\mathsf{S}}^{b\mathsf{c}} \tag{A4}$$

A3. Large Scale Component of MS-LETKF

The Kalman filter cost function for large scale component is constructed according to Li et al. (2012):

$$\begin{aligned} J_{\mathsf{L}}(\mathbf{x}_{\mathsf{L}}) = {} & (\mathbf{x}_{\mathsf{L}} - \bar{\mathbf{x}}_{\mathsf{L}}^{b})^{\mathsf{T}}(\mathbf{P}_{\mathsf{L}}^{b})^{-1}(\mathbf{x}_{\mathsf{L}} - \bar{\mathbf{x}}_{\mathsf{L}}^{b}) + [\mathbf{y}_{\mathsf{L}}^{o\mathsf{d}} - h^{\mathsf{d}}(\mathbf{x}_{\mathsf{L}})]^{\mathsf{T}}(\mathbf{R}_{\mathsf{L}}^{\mathsf{d}})^{-1}[\mathbf{y}_{\mathsf{L}}^{o\mathsf{d}} - h^{\mathsf{d}}(\mathbf{x}_{\mathsf{L}})] \\ & + [\mathbf{y}^{o\mathsf{c}} - h^{\mathsf{c}}(\mathbf{x}_{\mathsf{L}}) - \bar{\mathbf{y}}_{\mathsf{S}}^{b\mathsf{c}}]^{\mathsf{T}}[\mathbf{R}^{\mathsf{c}} + \tfrac{1}{(K-1)}\mathbf{Y}_{\mathsf{S}}^{b\mathsf{c}}(\mathbf{Y}_{\mathsf{S}}^{b\mathsf{c}})^{\mathsf{T}}]^{-1}[\mathbf{y}^{o\mathsf{c}} - h^{\mathsf{c}}(\mathbf{x}_{\mathsf{L}}) - \bar{\mathbf{y}}_{\mathsf{S}}^{b\mathsf{c}}] \end{aligned} \tag{A5}$$

where the additional term in the error covariance of coarse observation, $\frac{1}{(K-1)}\mathbf{Y}_{\mathsf{S}}^{b\mathsf{c}}(\mathbf{Y}_{\mathsf{S}}^{b\mathsf{c}})^{\mathsf{T}}$, is the representativeness error of small scale component. Through the transformation $\mathbf{x}_{\mathsf{L}} = \bar{\mathbf{x}}_{\mathsf{L}}^{b} + \mathbf{X}_{\mathsf{L}}^{b}\mathbf{w}_{\mathsf{L}}$ for large scale component, the Kalman filter cost function for large scale component is built in the ensemble space to assimilate both dense and coarse observations:

$$\begin{aligned} \tilde{J}_{\mathsf{L}}^{*}(\mathbf{w}_{\mathsf{L}}) = {} & (K-1)\mathbf{w}_{\mathsf{L}}^{\mathsf{T}}\mathbf{w}_{\mathsf{L}} + (\mathbf{y}_{\mathsf{L}}^{o\mathsf{d}} - \bar{\mathbf{y}}_{\mathsf{L}}^{b\mathsf{d}} - \mathbf{Y}_{\mathsf{L}}^{b}\mathbf{w}_{\mathsf{L}})^{\mathsf{T}}(\mathbf{R}_{\mathsf{L}}^{\mathsf{d}})^{-1}(\mathbf{y}_{\mathsf{L}}^{o\mathsf{d}} - \bar{\mathbf{y}}_{\mathsf{L}}^{b\mathsf{d}} - \mathbf{Y}_{\mathsf{L}}^{b\mathsf{d}}\mathbf{w}_{\mathsf{L}}) \\ & + (\mathbf{y}^{o\mathsf{c}} - \bar{\mathbf{y}}^{b\mathsf{c}} - \mathbf{Y}_{\mathsf{L}}^{b\mathsf{c}}\mathbf{w}_{\mathsf{L}})^{\mathsf{T}}[\mathbf{R}^{\mathsf{c}} + \tfrac{1}{(K-1)}\mathbf{Y}_{\mathsf{S}}^{b\mathsf{c}}(\mathbf{Y}_{\mathsf{S}}^{b\mathsf{c}})^{\mathsf{T}}]^{-1}(\mathbf{y}^{o\mathsf{c}} - \bar{\mathbf{y}}^{b\mathsf{c}} - \mathbf{Y}_{\mathsf{L}}^{b}\mathbf{w}_{\mathsf{L}}) \end{aligned} \tag{A6}$$

where $\bar{\mathbf{y}}^{b\mathsf{c}} = \mathbf{H}^{\mathsf{c}}\bar{\mathbf{x}}^{b} = \mathbf{H}^{\mathsf{c}}(\bar{\mathbf{x}}_{\mathsf{L}}^{b} + \bar{\mathbf{x}}_{\mathsf{S}}^{b}) = \bar{\mathbf{y}}_{\mathsf{L}}^{b\mathsf{c}} + \bar{\mathbf{y}}_{\mathsf{S}}^{b\mathsf{c}}$.

By minimizing the large scale Kalman filter cost function, we obtained

$$\tilde{\mathbf{P}}_{\mathsf{L}}^{a} = [(K-1)\mathbf{I} + (\mathbf{Y}_{\mathsf{L}}^{b\mathsf{d}})^{\mathsf{T}}(\mathbf{R}_{\mathsf{L}}^{\mathsf{d}})^{-1}(\mathbf{Y}_{\mathsf{L}}^{b\mathsf{d}}) + (\mathbf{Y}_{\mathsf{L}}^{b\mathsf{c}})^{\mathsf{T}}[\mathbf{R}^{\mathsf{c}} + \tfrac{1}{(K-1)}\mathbf{Y}_{\mathsf{S}}^{b\mathsf{c}}(\mathbf{Y}_{\mathsf{S}}^{b\mathsf{c}})^{\mathsf{T}}]^{-1}(\mathbf{Y}_{\mathsf{L}}^{b\mathsf{c}})]^{-1} \tag{A7}$$

$$\bar{\mathbf{w}}_{\mathsf{L}}^{a} = \tilde{\mathbf{P}}_{L}^{a}[(\mathbf{Y}_{\mathsf{L}}^{b\mathsf{d}})^{\mathsf{T}}(\mathbf{R}_{\mathsf{L}}^{\mathsf{d}})^{-1}(\mathbf{y}_{\mathsf{L}}^{o\mathsf{d}} - \bar{\mathbf{y}}_{\mathsf{L}}^{b\mathsf{d}}) + (\mathbf{Y}_{\mathsf{L}}^{b\mathsf{c}})^{\mathsf{T}}[\mathbf{R}^{\mathsf{c}} + \tfrac{1}{(K-1)}\mathbf{Y}_{\mathsf{S}}^{b\mathsf{c}}(\mathbf{Y}_{\mathsf{S}}^{b\mathsf{c}})^{\mathsf{T}}]^{-1}(\mathbf{y}^{o\mathsf{c}} - \bar{\mathbf{y}}^{b\mathsf{c}})] \tag{A8}$$

A4. Small Scale Component of MS-LETKF

For the small scale component, Li et al. (2012) utilized the information from large scale analysis, i.e. $\mathbf{y}_{\mathsf{L}}^{o\mathsf{d}} - \mathbf{H}^{\mathsf{d}}\bar{\mathbf{x}}_{\mathsf{L}}^{a} = \mathbf{y}_{\mathsf{L}}^{o\mathsf{d}} - \bar{\mathbf{y}}_{\mathsf{L}}^{a\mathsf{d}}$, to reduce undesirably large analysis increment at the surrounding points close to the dense observation area. In terms of Li et al. (2012), the Kalman filter cost function for small scale component

$$\begin{aligned} J_{\mathsf{S}}(\mathbf{x}_{\mathsf{S}}) = & (\mathbf{x}_{\mathsf{S}} - \bar{\mathbf{x}}_{\mathsf{S}}^{b})^{\mathsf{T}}(\mathbf{P}_{\mathsf{S}}^{b})^{-1}(\mathbf{x}_{\mathsf{S}} - \bar{\mathbf{x}}_{\mathsf{S}}^{b}) \\ & + [\mathbf{y}_{\mathsf{S}}^{o\mathsf{d}} - h^{\mathsf{d}}(\mathbf{x}_{\mathsf{S}}) + (\mathbf{y}_{\mathsf{L}}^{o\mathsf{d}} - \bar{\mathbf{y}}_{\mathsf{L}}^{a\mathsf{d}})]^{\mathsf{T}}[\mathbf{R}^{\mathsf{d}} + \tfrac{1}{(K-1)}\mathbf{Y}_{\mathsf{L}}^{a\mathsf{d}}(\mathbf{Y}_{\mathsf{L}}^{a\mathsf{d}})^{\mathsf{T}}]^{-1}[\mathbf{y}_{\mathsf{S}}^{o\mathsf{d}} - h^{\mathsf{d}}(\mathbf{x}_{\mathsf{S}}) + (\mathbf{y}_{\mathsf{L}}^{o\mathsf{d}} - \bar{\mathbf{y}}_{\mathsf{L}}^{a\mathsf{d}})] \\ & + [\mathbf{y}^{o\mathsf{c}} - h^{\mathsf{c}}(\mathbf{x}_{\mathsf{S}}) - \bar{\mathbf{y}}_{\mathsf{L}}^{b\mathsf{c}}]^{\mathsf{T}}[\mathbf{R}^{\mathsf{c}} + \tfrac{1}{(K-1)}\mathbf{Y}_{\mathsf{L}}^{b\mathsf{c}}(\mathbf{Y}_{\mathsf{L}}^{b\mathsf{c}})^{\mathsf{T}}]^{-1}[\mathbf{y}^{o\mathsf{c}} - h^{\mathsf{c}}(\mathbf{x}_{\mathsf{S}}) - \bar{\mathbf{y}}_{\mathsf{L}}^{b\mathsf{c}}] \end{aligned} \tag{A9}$$

could be constructed in ensemble space through the transformations of small scale part: $\mathbf{x}_{\mathsf{S}} = \bar{\mathbf{x}}_{\mathsf{S}}^{b} + \mathbf{X}_{\mathsf{S}}^{b}\mathbf{w}_{\mathsf{S}}$:

$$\begin{aligned} \tilde{J}_{\mathsf{S}}^{*}(\mathbf{w}_{\mathsf{S}}) = & (K-1)\mathbf{w}_{\mathsf{S}}^{\mathsf{T}}\mathbf{w}_{\mathsf{S}} \\ & + (\mathbf{y}^{o\mathsf{d}} - \bar{\mathbf{y}}_{\mathsf{S}}^{b\mathsf{d}} - \mathbf{Y}_{\mathsf{S}}^{b\mathsf{d}}\mathbf{w}_{\mathsf{S}} - \bar{\mathbf{y}}_{\mathsf{L}}^{a\mathsf{d}})^{\mathsf{T}}[\mathbf{R}^{\mathsf{d}} + \tfrac{1}{(K-1)}\mathbf{Y}_{\mathsf{L}}^{a\mathsf{d}}(\mathbf{Y}_{\mathsf{L}}^{a\mathsf{d}})^{\mathsf{T}}]^{-1}(\mathbf{y}^{o\mathsf{d}} - \bar{\mathbf{y}}_{\mathsf{S}}^{b\mathsf{d}} - \mathbf{Y}_{\mathsf{S}}^{b\mathsf{d}}\mathbf{w}_{\mathsf{S}} - \bar{\mathbf{y}}_{\mathsf{L}}^{a\mathsf{d}}) \\ & + (\mathbf{y}^{o\mathsf{c}} - \bar{\mathbf{y}}^{b\mathsf{c}} - \mathbf{Y}_{\mathsf{S}}^{b\mathsf{c}}\mathbf{w}_{\mathsf{S}})^{\mathsf{T}}[\mathbf{R}^{\mathsf{c}} + \tfrac{1}{(K-1)}\mathbf{Y}_{\mathsf{L}}^{b\mathsf{c}}(\mathbf{Y}_{\mathsf{L}}^{b\mathsf{c}})^{\mathsf{T}}]^{-1}(\mathbf{y}^{o\mathsf{c}} - \bar{\mathbf{y}}^{b\mathsf{c}} - \mathbf{Y}_{\mathsf{S}}^{b\mathsf{c}}\mathbf{w}_{\mathsf{S}}) \end{aligned} \tag{A10}$$

The solution of minimizing the Kalman filter cost function for small scale component is:

$$\tilde{\mathbf{P}}_{\mathsf{S}}^{a} = [(K-1)\mathbf{I} + (\mathbf{Y}_{\mathsf{S}}^{b\mathsf{d}})^{\mathsf{T}}[\mathbf{R}^{\mathsf{d}} + \tfrac{1}{(K-1)}\mathbf{Y}_{\mathsf{L}}^{a\mathsf{d}}(\mathbf{Y}_{\mathsf{L}}^{a\mathsf{d}})^{\mathsf{T}}]^{-1}(\mathbf{Y}_{\mathsf{S}}^{b\mathsf{d}}) + (\mathbf{Y}_{\mathsf{S}}^{b\mathsf{c}})^{\mathsf{T}}[\mathbf{R}^{\mathsf{c}} + \tfrac{1}{(K-1)}\mathbf{Y}_{\mathsf{L}}^{b\mathsf{c}}(\mathbf{Y}_{\mathsf{L}}^{b\mathsf{c}})^{\mathsf{T}}]^{-1}(\mathbf{Y}_{\mathsf{S}}^{b\mathsf{c}})]^{-1} \tag{A11}$$

$$\bar{\mathbf{w}}_{\mathsf{S}}^{a} = \tilde{\mathbf{P}}_{S}^{a}[(\mathbf{Y}_{\mathsf{S}}^{b\mathsf{d}})^{\mathsf{T}}[\mathbf{R}^{\mathsf{d}} + \tfrac{1}{(K-1)}\mathbf{Y}_{\mathsf{L}}^{a\mathsf{d}}(\mathbf{Y}_{\mathsf{L}}^{a\mathsf{d}})^{\mathsf{T}}]^{-1}(\mathbf{y}^{o\mathsf{d}} - \bar{\mathbf{y}}_{\mathsf{S}}^{b\mathsf{d}} - \bar{\mathbf{y}}_{\mathsf{L}}^{a\mathsf{d}}) + (\mathbf{Y}_{\mathsf{S}}^{b\mathsf{c}})^{\mathsf{T}}[\mathbf{R}^{\mathsf{c}} + \tfrac{1}{(K-1)}\mathbf{Y}_{\mathsf{L}}^{b\mathsf{c}}(\mathbf{Y}_{\mathsf{L}}^{b\mathsf{c}})^{\mathsf{T}}]^{-1}(\mathbf{y}^{o\mathsf{c}} - \bar{\mathbf{y}}^{b\mathsf{c}})] \tag{A12}$$

A5. Analysis in MS-LETKF

The large and small component of analysis ensemble mean and perturbation can be obtained by

$$\bar{\mathbf{x}}_{\mathsf{L}}^{a} = \bar{\mathbf{x}}_{\mathsf{L}}^{b} + \mathbf{X}_{\mathsf{L}}^{b}\bar{\mathbf{w}}_{\mathsf{L}}^{a} \tag{A13}$$

$$\mathbf{X}_{\mathsf{L}}^{a} = \mathbf{X}_{\mathsf{L}}^{b}[(K-1)\tilde{\mathbf{P}}_{\mathsf{L}}^{a}]^{1/2} \tag{A14}$$

$$\bar{\mathbf{x}}_{\mathsf{S}}^{a} = \bar{\mathbf{x}}_{\mathsf{S}}^{b} + \mathbf{X}_{\mathsf{S}}^{b}\bar{\mathbf{w}}_{\mathsf{S}}^{a} \tag{A15}$$

$$\mathbf{X}_{\mathsf{S}}^{a} = \mathbf{X}_{\mathsf{S}}^{b}[(K-1)\tilde{\mathbf{P}}_{\mathsf{S}}^{a}]^{1/2} \tag{A16}$$

The analysis of the kth ensemble member is the sum of large and small components of it

$$\begin{aligned} \mathbf{x}^{a(k)} &= \mathbf{x}_{\mathsf{L}}^{a(k)} + \mathbf{x}_{\mathsf{S}}^{a(k)} \\ &= \bar{\mathbf{x}}_{\mathsf{L}}^{a} + \mathbf{X}_{\mathsf{L}}^{a(k)} + \bar{\mathbf{x}}_{\mathsf{S}}^{a} + \mathbf{X}_{\mathsf{S}}^{a(k)} \end{aligned} \tag{A17}$$

REFERENCES

Anderson, J. L., 2007: An adaptive covariance inflation error correction algorithm for ensemble filters. *Tellus A*, **59**, 210–224.

Anderson, J. L., 2009: Spatially and temporally varying adaptive covariance inflation for ensemble filters. *Tellus A*, **61**, 72–83.

Anderson, J. L. and S. L. Anderson, 1999: A monte carlo implementation of the nonlinear filtering problem to produce ensemble assimilations and forecasts. *Mon. Wea. Rev.*, **127**, 2741–2758.

Arakawa, A. and V. R. Lamb, 1977: Computational design of the basic dynamical process of the ucla general circulation model. *Meth. Comput. Phys.*, **17**, 173–265.

Blaas, M., C. Dong, P. Marchesiello, J. C. McWilliams, and K. D. Stolzenbach, 2007: Sediment-transport modeling on Southern Californian shelves: A ROMS case study. *Cont. Shelf Res.*, **27 (6)**, 832–853, doi:10.1016/j.csr.2006.12.003.

Capet, X., J. C. McWilliams, M. J. Molemaker, and A. F. Shchepetkin, 2008a: Mesoscale to submesoscale transition in the california current system. part i: Flow structure, eddy flux, and observational tests. *J. Phys. Oceanogr.*, **38**, 29–43.

Capet, X., J. C. McWilliams, M. J. Molemaker, and A. F. Shchepetkin, 2008b: Mesoscale to submesoscale transition in the california current system. part ii: Frontal processes. *J. Phys. Oceanogr.*, **38**, 44–64.

Capet, X., J. C. McWilliams, M. J. Molemaker, and A. F. Shchepetkin, 2008c: Mesoscale to submesoscale transition in the california current system. part iii: Energy balance and flux. *J. Phys. Oceanogr.*, **38**, 2256–2269.

Capet, X. J., P. Marchesiello, and J. C. McWilliams, 2004: Upwelling response to coastal wind profiles. *Geophys. Res. Lett.*, **31 (13)**, 1–4, doi:10.1029/2004GL020123.

Chao, Y., et al., 2009: Development, implementation and evaluation of a data-assimilative ocean forecasting system off the central california coast. *Deep-sea Res. II*, **56**, 100–126.

Cummings, J. A., 2005: Operational multivariate ocean data assimilation. *Q. J. R. Meteorol. Soc.*, **131**, 3583–3604.

Derver, J. and F. Bouttier, 1999: A reformulation of the background error covariance in the ecmwf global data assimilation system. *Tellus A*, **51**, 195–221.

Greybush, S. J., E. Kalnay, T. Miyoshi, K. Ide, and B. R. Hunt, 2011: Balance and ensemble kalman filter localization techniques. *Mon. Wea. Rev.*, **139**, 511–522.

Gruber, N., et al., 2006: Eddy-resolving simulation of plankton ecosystem dynamics in the California Current System. *Deep. Res. Part I Oceanogr. Res. Pap.*, **53 (9)**, 1483–1516, doi:10.1016/j.dsr.2006.06.005.

Hacker, J. P., J. L. Anderson, and M. Pagowski, 2007: Improved vertical covariance estimates for ensemble-filter assimilation of near-surface observations. *Mon. Wea. Rev.*, **135**, 1021–1036.

Hamill, T. M., J. S. Whitaker, and C. Snyder, 2001: Distance-dependent filtering of background error covariance estimates in an ensemble kalman filter. *Mon. Wea. Rev.*, **129**, 2776–2790.

Hoffman, M. J., T. Miyoshi, T. W. N. Haine, K. Ide, C. W. Brown, and R. Murtugudde, 2012: An advanced data assimilation system for the chesapeake bay: Performance evaluation. *J. Atmos. Ocean. Tech.*, **29**, 1542–1557.

Houtekamer, P. L., H. K. Mitchell, and X. Deng, 2009: Model error representation in an operational ensemble kalman filter. *Mon. Wea. Rev.*, **137**, 2126–2143.

Houtekamer, P. L. and H. L. Mitchell, 1998: Data assimilation using an ensemble kalman filter technique. *Mon. Wea. Rev.*, **126**, 796–811.

Houtekamer, P. L., H. L. Mitchell, G. Pellerin, M. Buehner, M. Charron, L. Spacek, and B. Hansen, 2005: Atmospheric data assimilation with an ensemble kalman filter: Results with real observation. *Mon. Wea. Rev.*, **133**, 604–620.

Hunt, B. R., E. J. Kostelich, and I. Szunyogh, 2007: Efficient data assimilation for spatiotemporal chaos: A local ensemble transform kalman filter. *Physica D*, **230**, 112–126.

Ide, K., P. Courtier, M. Ghil, and A. Lorenc, 1997: Unified notation for data assimilation: Operational, sequential and variational. *J. Meteor. Soc. Japan*, **75**, 181–189.

Kang, J.-S., E. Kalnay, J. Liu, I. Fung, T. Miyoshi, and K. Ide, 2011: "variable localization" in an ensemble kalman filter: Application to the carbon cycle data assimilation. *J. Geophys. Res.*, **116**, doi:10.1029/2010JD014673.

Kara, A. B., P. A. Rochford, and H. E. Hurlburt, 2000: An optimal definition for ocean mixed layer depth. *J. Geophys. Res.*, **105**, 16 803–16 821.

Keppenne, C. L., 2000: Data assimilation into a primitive-equation model with a parallel ensemble kalman filter. *Mon. Wea. Rev.*, **128**, 1971–1981.

Keppenne, C. L. and M. M. Rienecker, 2002: Initial testing of a massively parallel ensemble kalman filter with the poseidon isopycnal ocean general circulation model. *Mon. Wea. Rev.*, **130**, 2951–2965.

Large, W. G., J. C. McWilliams, and S. C. Doney, 1994: Oceanic vertical mixing: A review and a model with a nonlocal boundary layer parameterization. *Rev. Geophys.*, **32 (4)**, 363, doi:10.1029/94RG01872.

Li, H., E. Kalnay, and T. Miyoshi, 2009: Simultaneous estimation of covariance inflation

and observation errors within an ensemble kalman filter. *Quart. J. Roy. Meteor. Soc.*, **135**, 523–533.

Li, Z., Y. Chao, J. C. McWillams, K. Ide, and J. Farrara, 2012: A multi-scale three-dimensional variational data assimilation scheme and its application to coastal oceans. *Quart. J. Roy. Meteor. Soc.*, [submitted].

Li, Z., Y. Chao, J. C. McWilliams, and K. Ide, 2008: A three-dimensional variational data assimilation scheme for the regional ocean modeling system. *J. Atmos. Oceanic Technol.*, **25**, 2074–2090.

Marchesiello, P., J. C. McWilliams, and A. Shchepetkin, 2001: Open boundary conditions for long-term integration of regional oceanic models. *Ocean Model.*, **3**, 1–20, doi:10.1016/S1463-5003(00)00013-5.

Marchesiello, P., J. C. McWilliams, and A. F. Shchepetkin, 2003: Equilibrium Structure and Dynamics of the California Current System. *J. Phys. Oceanogr.*, **33 (4)**, 753–783, doi:10.1175/1520-0485(2003)33⟨753:ESADOT⟩2.0.CO;2, URL `http://dx.doi.org/10.1175/1520-0485(2003)33{\textless}753:ESADOT{\textgreater}2.0.CO;2`.

Miyoshi, T., 2011: The gaussian approach to adaptive covariance inflation and its implementation with the local ensemble transform kalman filter. *Mon. Wea. Rev.*, **139**, 1519–1535.

Miyoshi, T., K. Ide, J. McWilliams, G. Li, Y. Uchiyama, and E. Kalnay, 2010: Ensemble data assimilation for idealized california current system with roms-letkf. URL `www.cawcr.gov.au/staff/pxs/wmoda5/ExtendedAbstracts/Miyoshi_etal_a.pdf`.

Miyoshi, T. and M. Kunii, 2012: Wrf-letkf: The present and beyond. URL `http://www.weatherchaos.umd.edu/group_log/index.html`.

Ott, E., et al., 2004: A local ensemble kalman filter for atmospheric data assimilation. *Tellus A*, **56**, 415–428.

Patil, D. J., B. R. Hunt, E. Kalnay, J. A. Yorke, and E. Ott, 2001: Local low dimensionality of atmospheric dynamics. *Phys. Rev. Lett.*, **86**, 5878–5881.

Penny, S. G., E. Kalnay, J. A. Carton, B. Hunt, K. Ide, T. Miyoshi, and G. A. Chepurin, 2013: The local ensemble transform kalman filter and the running-in-place algorithm applied to a global ocean general circulation model. *Nonlin. Processes Geophys.*, **20**, 1031–1046.

Ricci, S., A. T. Weaver, J. Vialard, and P. Rogel, 2005: Incorporating state-dependent temperature-salinity constraints in the background error covariance of variational ocean data assimilation. *Mon. Wea. Rev.*, **133**, 317–338.

Shchepetkin, A. F. and J. C. McWilliams, 2003: A method for computing horizontal pressure-gradient force in an oceanic model with a non-aligned vertical coordinate. *J. Geophys. Res.*, **108**, 3090.

Shchepetkin, A. F. and J. C. McWilliams, 2005: The regional oceanic modeling system (roms): A split-explicit, free-surface, topography-following-coordinate ocean model. *Ocean Modell.*, **9**, 347–404.

Shchepetkin, A. F. and J. C. McWilliams, 2008: Computational kernel algorithms for fine-scale, multi-process, long-time oceanic simulations. *Handb. Numer. Anal. Spec. Vol. Comput. Methods Atmos. Ocean.*, **14**, 121–183, doi:10.1016/S1570-8650(08)01202-0.

Shulman, I. and J. D. Paduan, 2009: Assimilation of hf radar-derived radials and total currents in the monterey bay area. *Deep-Sea Research II*, **56**, 149–160.

Troccoli, A., et al., 2002: Salinity adjustments in the presence of temperature data assimilation. *Mon. Wea. Rev.*, **130**, 89–102.

Weaver, A. T., C. Deltel, E. Machu, S. Ricci, and N. Daget, 2005: A multivariate balance operator for variational ocean data assimilation. *Q. J. R. Meteorol. Soc.*, **131**, 3605–3625.

Whitaker, J. S., G. P. Compo, X. Wei, and T. M. Hamill, 2004: Reanalysis without radiosondes using ensemble data assimilation. *Mon. Wea. Rev.*, **132**, 1190–1200.

Whitaker, J. S., T. M. Hamill, X. Wei, Y. Song, and Z. Toth, 2008: Ensemble data assimilation with the ncep global forecast system. *Mon. Wea. Rev.*, **136**, 463–482.

Zhang, F., C. Snyder, and J. Sun, 2004: Impacts of initial estimate and observation availability on convective-scale data assimilation with ensemble kalman filter. *Mon. Wea. Rev.*, **132**, 1238–1253.